VETOR

Electrochemical Characterization of Amorphous and Crystalline $Ni_{62}Nb_{38}$ and $Ni_{59.24}Nb_{37.76}B_{3.00}$ Alloys

Caracterização Eletroquímica das Ligas $Ni_{62}Nb_{38}$ e $Ni_{59.24}Nb_{37.76}B_{3.00}$ Com Estruturas Amorfas e Cristalinas

Emandro Vieira da Costa[1], Marcelo Lemos da Silva[1], Marcos Paulo Moura de Carvalho[1], Daniel Magalhães da Cruz[2], Luis César Rodríguez Aliaga, [1] Ivan Napoleão Bastos[1,†]

[1]*Instituto Politécnico, Universidade do Estado do Rio de Janeiro, Nova Friburgo, Brasil*

[2]*Federal University of Rio Grande do Sul, Porto Alegre, Brasil*

[†]**Corresponding author:** inbastos@iprj.uerj.br

Abstract

Nickel-based alloys are widely used in industry due to their remarkable corrosion resistance. Currently, most of these alloys are processed with crystalline structure. However, amorphous metal alloys commonly demonstrate greater corrosion resistance compared to their crystalline counterparts. In this study, the $Ni_{62}Nb_{38}$, $Ni_{59.24}Nb_{37.76}B_{3.00}$, and $Ni_{58.1}Nb_{38.9}B_{3.0}$ (atom percent) alloys with crystalline and amorphous structure were investigated. Traditional X-ray diffraction (XRD) and differential scanning calorimetry (DSC) techniques were used to characterize the alloys. Electrochemical tests were conducted to evaluate the corrosion resistance at different temperatures. Data obtained by electrochemical impedance spectroscopy and polarization curves revealed the superiority of amorphous alloys in relation to crystalline ones, for the same chemical composition. The polarization resistance of the amorphous alloys was up to 20 times greater than that of its crystalline counterparts. Both structures showed a reduction in corrosion resistance with increasing temperature. In amorphous alloys, the presence of boron made the samples more resistant to corrosion at both temperatures. Furthermore, a higher percentage of niobium among the ternary compositions also improved the corrosion properties. In crystalline alloys, the presence of boron resulted in samples that were less resistant to corrosion at a temperature of 25 °C. However, this element provided greater resistance to ternary alloys at a temperature of 45 °C. Using electrochemical techniques, it was possible to demonstrate the superior corrosion resistance of amorphous alloys compared to its crystalline counterparts.

Keywords

Amorphous Ni-Nb-based Alloys • Electrochemical characterization • Corrosion resistance

Resumo

Ligas à base de níquel são amplamente utilizadas na indústria devido à sua notável resistência à corrosão. Atualmente, a maioria dessas ligas é processada com estrutura cristalina. Entretanto, as ligas metálicas amorfas, comumente, demonstram uma maior resistência à corrosão em comparação com suas contrapartes cristalinas. Neste estudo, foram investigadas ligas metálicas $Ni_{62}Nb_{38}$, $Ni_{59,24}Nb_{37,76}B_{3,00}$ e $Ni_{58,1}Nb_{38,9}B_{3,0}$ (percentagem atômica), com estruturas cristalina e amorfa. Utilizou-se difração de raios-X (DRX) e calorimetria diferencial de varredura (DSC) para análise das ligas. Os testes eletroquímicos foram conduzidos para avaliar a resistência à corrosão em diferentes temperaturas. Os dados obtidos por espectroscopia de impedância eletroquímica e curvas de polarização revelaram a superioridade das ligas amorfas em relação às cristalinas, para uma mesma composição química. A

resistência de polarização da liga amorfa foi até 20 vezes maior que a de sua contraparte cristalina. Ambas as estruturas mostraram uma redução na resistência à corrosão com o aumento da temperatura. Nas ligas amorfas, a presença de boro tornou as amostras mais resistentes à corrosão em ambas as temperaturas. Além disso, o maior percentual de nióbio entre as composições ternárias também melhorou as propriedades em relação à corrosão. Nas ligas cristalinas, a presença de boro resultou em amostras menos resistentes à corrosão à temperatura de 25 °C. No entanto, esse elemento proporcionou uma maior resistência das ligas ternárias à temperatura de 45 °C. Utilizando técnicas eletroquímicas, foi possível demonstrar a superioridade da resistência à corrosão das ligas amorfas em comparação com as cristalinas, para uma mesma composição química.

Palavras-chave

Ligas Amorfas de Ni-Nb • Caracterização eletroquímica • Resistência à corrosão

1 Introduction

The development of new metallic alloys is constantly necessary when technological and industrial advances occur. Those improved materials provide superior properties to those currently known [1]. Among them, the amorphous metallic alloys have been gaining prominence in scientific research [2]. One of the main advantages of amorphous metallic alloys is the greater resistance to corrosion than their crystalline counterparts [3], which is crucial in several areas of industry, where the entire process depends on the reliability of these components [4].

However, in certain cases, when comparing the same chemical composition of an alloy in two different forms, the crystalline structure demonstrates superior resistance to corrosion [5]. Additionally, the properties that determine the corrosion resistance of amorphous alloys tend to be highly sensitive to their chemical composition. Therefore, the investigation of different compositions of amorphous alloys is extremely relevant.

In some industrial applications, where the metal alloy will be exposed to extremely aggressive environments, such as chemical, petrochemical and food processing industries, nickel-based alloys are widely used [6]. Environments where conventional stainless-steel alloys and stainless superalloys would not be suitable [7]. Although the literature presents numerous studies on nickel-based alloys in their crystalline form [8], there are a significant small number of papers available focused on the investigation of the same alloys in its amorphous form.

This study aims to apply X-ray diffraction (XRD), differential scanning calorimetry (DSC) and electrochemical techniques to characterize Ni-Nb and Ni-Nb-B system alloys, covering both crystalline and amorphous structures. The study will be conducted in an environment simulating seawater conditions (3.5% NaCl). Furthermore, investigate the behavior of corrosion resistance for different compositions in amorphous arrangements, and later compare them to their respective compositions in crystalline form.

2 Materials and methods

For the development of the samples, nickel (99.99% purity), niobium (99.99% purity) and boron (99.9% purity) were used, all acquired through Alfa Aesar (USA). To obtain the desired metallic alloys, two processing steps of melting and solidification were used. In the first stage, pure elements were melted to form a crystalline alloy. In the second stage, these metallic alloys with a crystalline structure were remelted and quickly solidified to obtain an amorphous structure.

2.1 Obtaining Crystalline and Amorphous Metallic Alloys

All alloying components were meticulously treated and inspected at each stage of the process, aiming to eliminate any traces of oxidation, oil residues or impurities. There was constant attention to the mass of each element, ensuring that it resulted in the desired chemical composition at the end of the entire procedure.

The following step was the producing of crystalline metallic alloys, using the arc-melting technique under high purity Ar atmosphere and Ti-getter. The process was repeated several times until obtaining a chemically homogeneous and crystalline alloy. Three alloys were developed with their respective chemical compositions described in Table 1.

To produce amorphous alloys, the melt-spinning technique was used. As a base material to start the process, crystalline alloys previously obtained by arc-melting were used. Spun ribbons with a thickness of approximately 25 μm, an average width of 3 mm and a length of approximately 10 m were produced. To facilitate the presentation of alloys throughout the work, the following terms were adopted: The binary $Ni_{62}Nb38$ amorphous alloy, was

termed as alloy A, and the ternary amorphous alloys with the presence of boron termed as B and C alloys. The symbols of crystalline structure have the superscript ^{c}, as shown in Table 1.

Table 1: Chemical composition of the alloys.

Alloy		**Chemical Composition**	
amorphous	**crystalline**	**atom %**	**mass %**
A	A^{c}	$Ni_{62}Nb_{38}$	$Ni_{50.75}Nb_{49.25}$
B	B^{c}	$Ni_{59.24}Nb_{37.76}B_{3.00}$	$Ni_{49.55}Nb_{49.99}B_{0.46}$
C	C^{c}	$Ni_{58.10}Nb_{38.90}B_{3.00}$	$Ni_{48.32}Nb_{51.22}B_{0.46}$

To confirm the crystalline and the amorphous structures of the samples, the XRD and DSC techniques were used. It should be noted that the XRD technique offers structural information paying attention to the number of type of phases present in the sample, however, the DSC is related mainly to the thermal behavior of the materials providing information about the temperatures of phase transformations. Further details regarding these tests are presented in the results and discussions sections.

2.2 Preparation of Samples for Electrochemical Tests

To the electrochemical tests of crystalline samples, each of the three alloys obtained were embedded in acrylic resin leaving only one side exposed, thus the rest of the part was electrically isolated, as displayed in Figure 1(a). In case of the amorphous ribbons the measured length, Figure 1(b), they were complete immersed in the electrolyte. Before each test, the samples were sanded with 100, 300, and 600 grit sandpaper. The exposed area of crystalline samples was 0.335 cm^2. For the amorphous alloy samples, the width of the ribbon was measured using a caliper, and the length was established so that the resulting area (considering both sides) was 1.0 cm^2. This resulted in specimens ranging from 50 to 70 mm, with an increase of approximately 20 mm to ensure the viability of electrical contact.

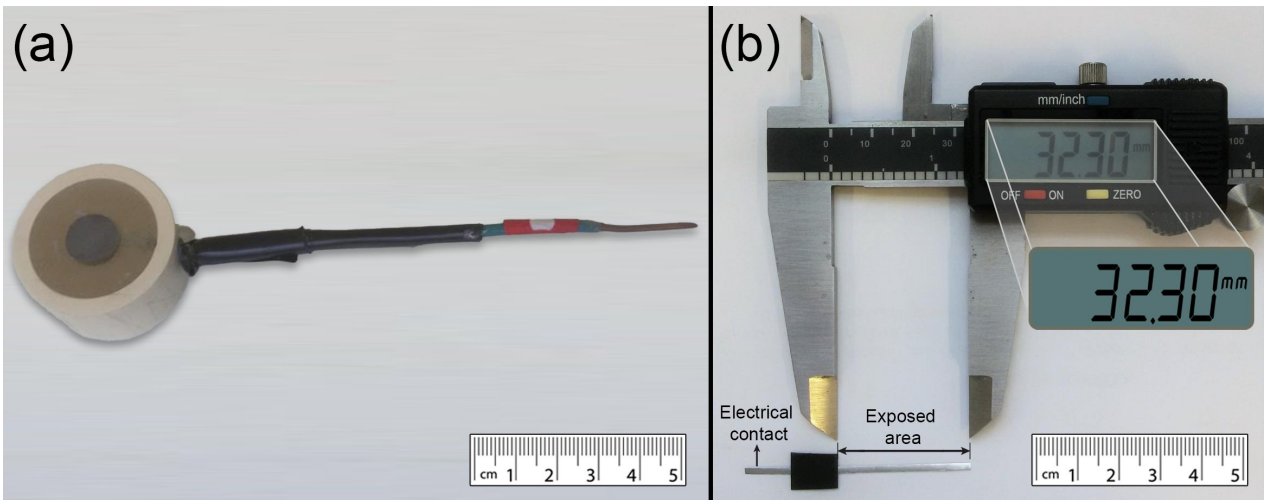

Figure 1: (a) Crystalline alloy samples (b) Amorphous alloy samples

For all electrochemical tests, the electrolyte used was an aqueous solution containing 3.5% mass of NaCl, allowing the simulation of the behavior of the alloys in seawater. The temperature of the solution was regulated by a thermostat, establishing temperatures of 25 °C and 45 °C as the temperatures for the tests. A Gamry Instruments potentiostat, model Reference 600, was used. The saturated calomel electrode (SCE) was used as the reference electrode and a spiral platinum wire as the counter electrode (CE). For each condition, three tests were conducted, aiming to eliminate any unwanted variations.

3 Results and Discussions

In this section, the characterization of the samples by using both XRD and DSC techniques are presented, followed by the results of the electrochemical tests.

3.1 X-ray Diffraction

Figure 2 exhibits the X-ray diffractograms corresponding to the crystalline and amorphous samples. The presence of well-defined peaks reveals the crystalline structure of the A^c, B^c, and C^c alloys. In the A^c (binary) alloy, the presence of the $NbNi_3$ and NbNi phases can be observed, while in the B^c and C^c (ternary) alloys, the intermetallic $NbNi_3$, NbNi, and NbB were identified.

Even though it is not predicted by the equilibrium phase diagrams, the presence of NbNi in the XRD results is due to the relatively fast cooling kinetics obtained in the arc-melting method in water cooled cooper crucible used in processing the crystalline samples. Thus, the cooling rates are high enough to form that intermetallic in a metastable state.

Regarding to vitreous metals, it is possible to identify for the three compositions, the presence of a diffuse halo that is characteristic of the amorphous phase [9]. No peaks related to crystalline phases were observed. Furthermore, small peaks at low angles typical of the substrate diffraction can also be noticed through the XRD, corresponding to the polymer in the sample holder. The small crystalline peak observed at 18° in the amorphous ternary alloy containing 59.24% nickel (alloy B) can be attributed to the influence of the support.

The diffuse halos of the three amorphous alloys are distributed over a range of angles of approximately 38 to 50°, which, in crystalline samples, is where most of the peaks are located. In a study on the formation of binary amorphous alloys of the Ni-Nb system [10], similar diffractograms were obtained.

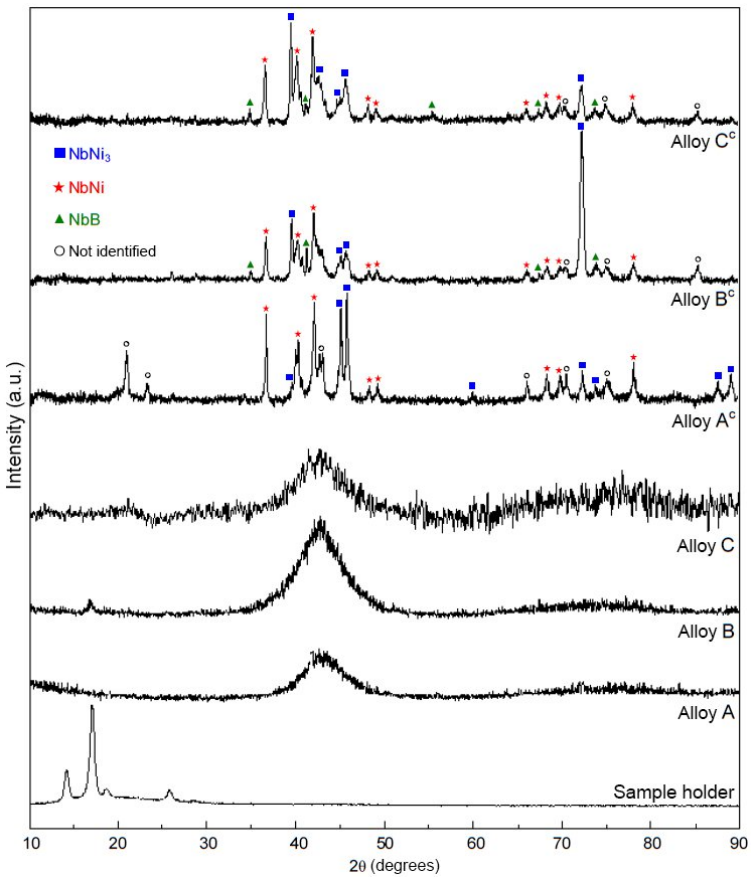

Figure 2: X-ray diffractograms corresponding to crystalline and amorphous samples.

3.2 Thermal analysis

The DSC thermograms of the amorphous ribbons obtained at heating rate of 40 °C.min^{-1} are shown in Figure 3. It is possible to observe that there are several phase transformations depending on the chemical composition of the samples. Alloy A (binary) presents a broad structural relaxation that is confused with the glass transition, however, samples with 3% boron present a well-defined glass transition (Tg), followed by thermal crystallization (Tx) that occurs in two stages for alloy C, and in just a single event for alloy B. The presence of boron increased the crystallization temperature of alloys B and C ($T_{x,B}$ and $T_{x,C}$) causing, therefore, an increase in the supercooled liquid region ($\Delta Tx = Tx - Tg$) of these alloys. While alloy A presented $\Delta T_{x,A} = 34$ °C, for alloys B and C these values were, respectively, $\Delta T_{x,B} = 55$ °C and $\Delta T_{x,C} = 49$ °C. In this way, the presence of boron contributed to the formation of the amorphous structure, increasing the glass forming ability (GFA) of the B and C alloys. This result is corroborated by the literature in which elements such as B and Ni are normally used to increase the tendency to form amorphous metal [9]. The DSC curves also showed two crystallization peaks at temperatures of 675 and 725 °C. The supercooled liquid region presented a slightly wider temperature range, equal to 40 °C, while in this work the estimated value was 34 °C. This small difference may be a consequence of different methods used to calculate the glass transition and crystallization temperatures. On the other hand, it is important to highlight that although ternary amorphous alloys have the same boron content, the amorphous structure at the level of clusters may be different as the DSC curves show very different thermal behavior. It is expected that the corrosion behavior also be sensible to the structures.

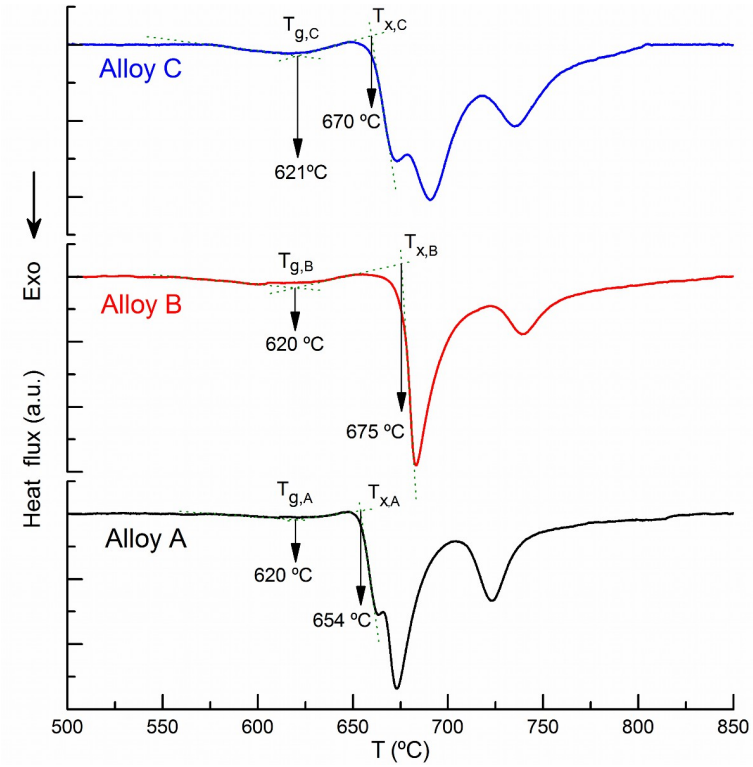

Figure 3: DSC thermograms at the heating rate of 40 °C.min^{-1} to determine the thermal parameters corresponding to the amorphous phase.

3.3 Open Circuit Potential

The open circuit potential curves of crystalline and amorphous alloys at 25 and 45 °C are shown in Figure 4. Observing the curves generated for tests carried out at 25 °C, a large difference is observed between the potentials reached by crystalline and amorphous samples after 10 hours of immersion in the electrolyte. While crystalline alloys reached potentials close to – 325 mV SCE, glassy metals reached values around –185 mV SCE. Thus, one can infer the greater reactivity of the crystalline structures, reaching stability more quickly, and reaching lower potential values after 10 hours in open circuit.

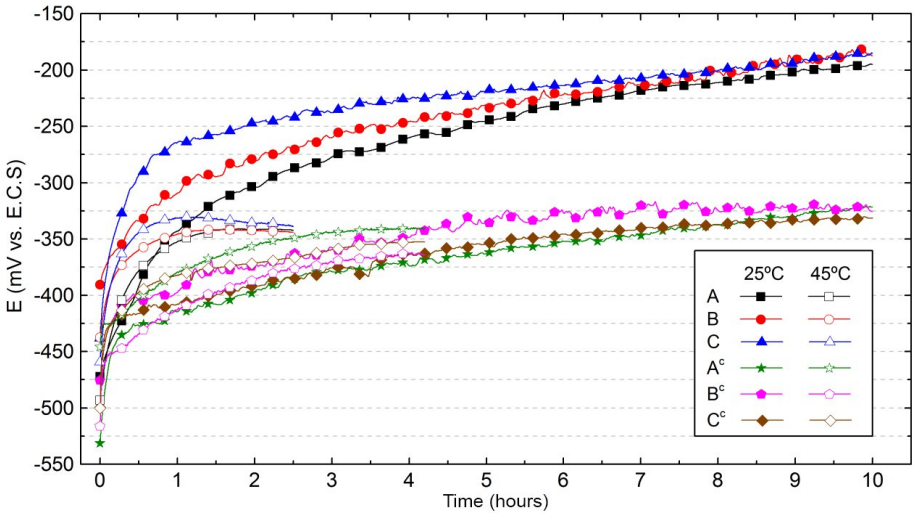

Figure 4: Open circuit potential curves of crystalline and amorphous samples at 25 and 45 °C

Raising the temperature to 45 °C significantly increased the stabilization speed of passive films. In amorphous alloys, this temperature increases drastically reduced the time required for the potential values to stabilize to the point where variations become insignificant enough to consider the system stable and define the corrosion potential. Crystalline alloys, in contrast, showed less sensitivity to increased temperature in relation to open circuit time.

3.4 Potentiodynamic Polarization

Figure 5 shows the polarization curves at 25 and 45 °C of the studied samples. Initially, it can be observed that all samples present a wide range of potentials in which the current density remains constant, characterizing a passive region due to the film formed. A similar behavior in the polarization of amorphous metallic alloys was obtained by others [11,12]. In agreement with the results of the open circuit potential curves, the potentiodynamic polarization of the samples confirms that for the same chemical composition, the crystalline structure presents greater reactivity than the amorphous one. When compared for the same potential value, crystalline alloys showed higher corrosion current density than amorphous alloys.

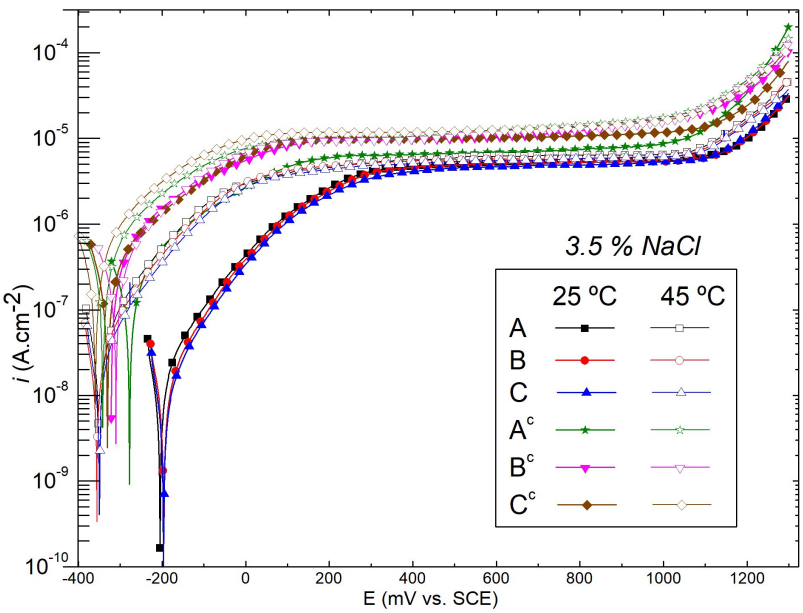

Figure 5: Potentiodynamic polarization curves of crystalline and amorphous samples at 25 and 45 °C

When the corrosion potential (E_{corr}) is evaluated at 25 °C, glassy metals showed higher potentials than their crystalline counterparts. However, when the temperature is raised to the 45 °C. The E_{corr} values of both structures were similar. The amorphous alloys tested at 25 °C showed corrosion potentials close to -200 mV SCE, while at 45 °C the potentials of these alloys reduce to values close to -350 mV SCE. This behavior is expected since increasing temperature tends to favor the kinetics of reactions. Furthermore, the dissolved oxygen content reduces with temperature, and thus tends to reduce the measured potential. Consequently, it is observed that at 45 °C non-crystalline samples reach the passivation region more easily, around -200 mV SCE. In crystalline alloys, however, this effect occurs with less intensity.

The i_{pass} passivation current density values are displayed in Figure 6 and were determined to be the current value at a potential equal to 700 mV SCE for the amorphous alloys tested at 25 °C, and 600 mV SCE for the other tests. As observed in the polarization curves, the i_{pass} values of amorphous alloys are considerably lower than those of crystalline alloys. Furthermore, observing the Figure 6 it is very evident that higher temperature increases the passivation current density for both structures, in accordance with results available in the literature [13,14].

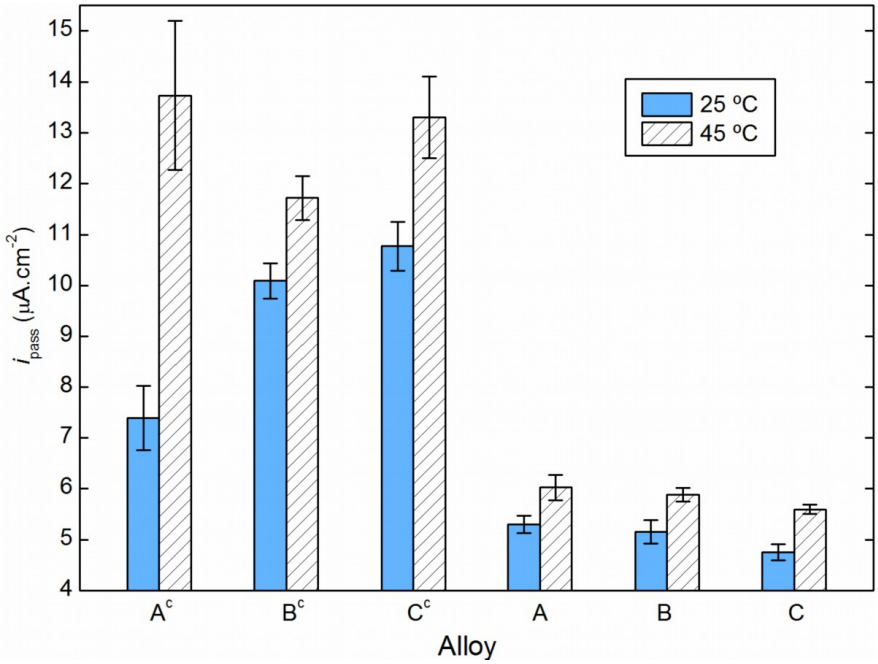

Figure 6: Passivation current density of crystalline and amorphous alloys at 25 and 45 ºC. (Average of three samples)

The passivation current density increases from binary to ternary alloy, at both temperatures, in the amorphous condition. At 25 °C, the trend is reversed towards the crystalline structure. Among the glassy alloys, the binary alloy (alloy A) has the highest i_{pass} values, both temperatures at 25 °C and 45 °C, indicating lower corrosion resistance of this sample in relation to another amorphous alloys. Among the crystalline alloys, the opposite occurred at 25 °C, that is, the composition without the presence of boron was the one with the lowest value of passivation current, proving to be more resistant to corrosion than the B^c and C^c alloys of the Ni-Nb-B system. This behavior can be explained by the presence of boron, which results in a structure with a higher fraction of intermetallic compounds, making the surface of the B^c and C^c alloys more heterogeneous, with a greater number of grain boundaries and, probably, less resistant to corrosion than the alloy A^c. On the other hand, at 45 °C, the passivation current of the $Ni_{62}Nb_{38}$ alloy, with a crystalline structure, was greater than that of the crystalline alloys $Ni_{59.24}Nb_{37.76}B_{3.00}$, and $Ni_{58.1}Nb_{38.9}B_{3.0}$. This result suggests that, although the presence of boron makes the microstructure of crystalline alloys more heterogeneous, this element can be important in applications where working temperatures are above 25 °C.

3.5 Electrochemical Impedance Spectroscopy

The electrochemical impedance spectra and the graphical results of the equivalent circuit adjustments are presented using the Nyquist (Figure 7) and Bode (Figure 8) diagrams. In the Nyquist diagram, all samples are included at temperatures of 25 °C and 45 °C (the impedance modules of the crystalline alloys were multiplied by 2 for better

visualization of the information). The Bode diagram shows the results of binary alloys, in the amorphous and crystalline state, at 25 and 45 °C.

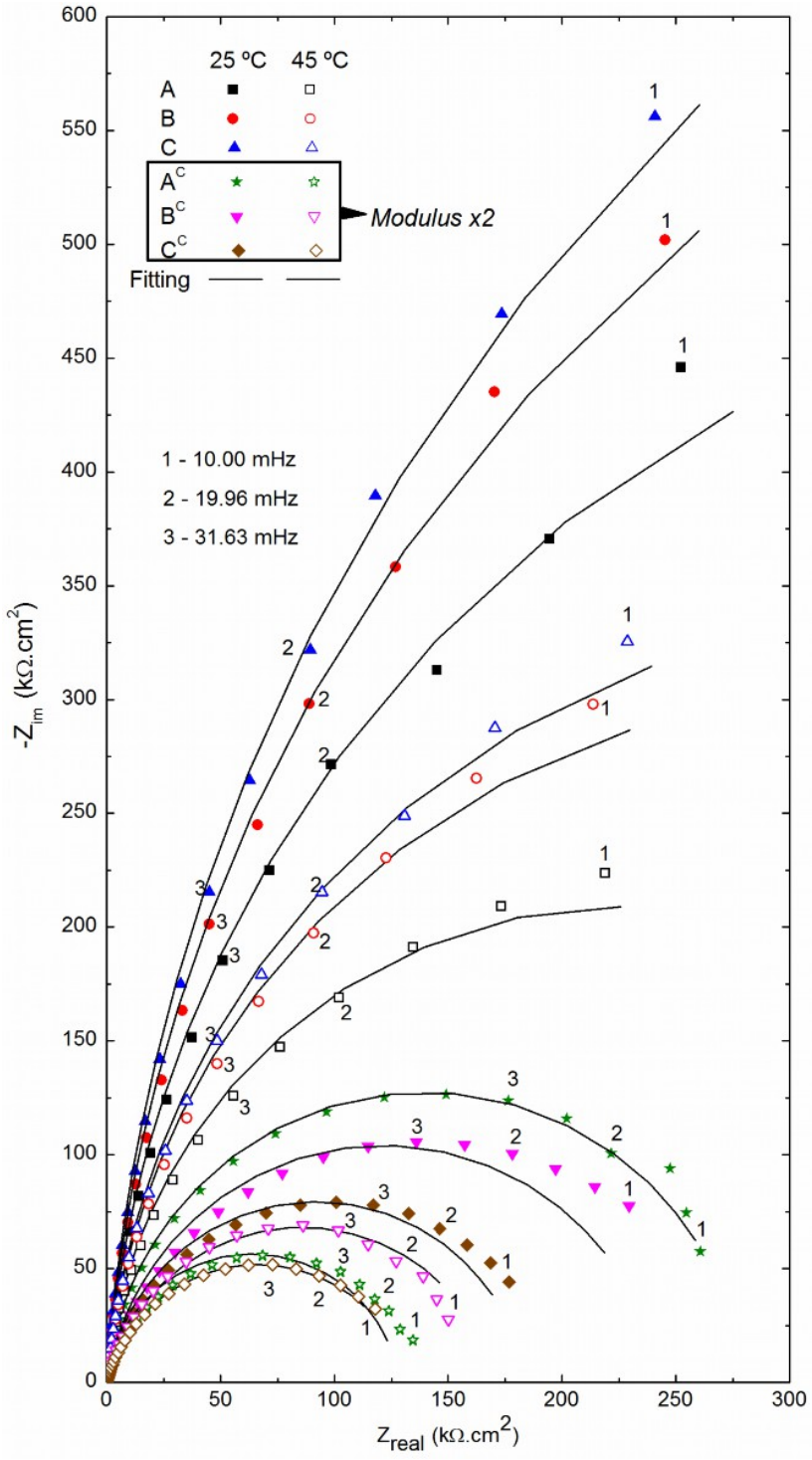

Figure 7: Nyquist diagrams and fitted curves equivalent electrical circuit of the crystalline and amorphous samples at 25 and 45 °C

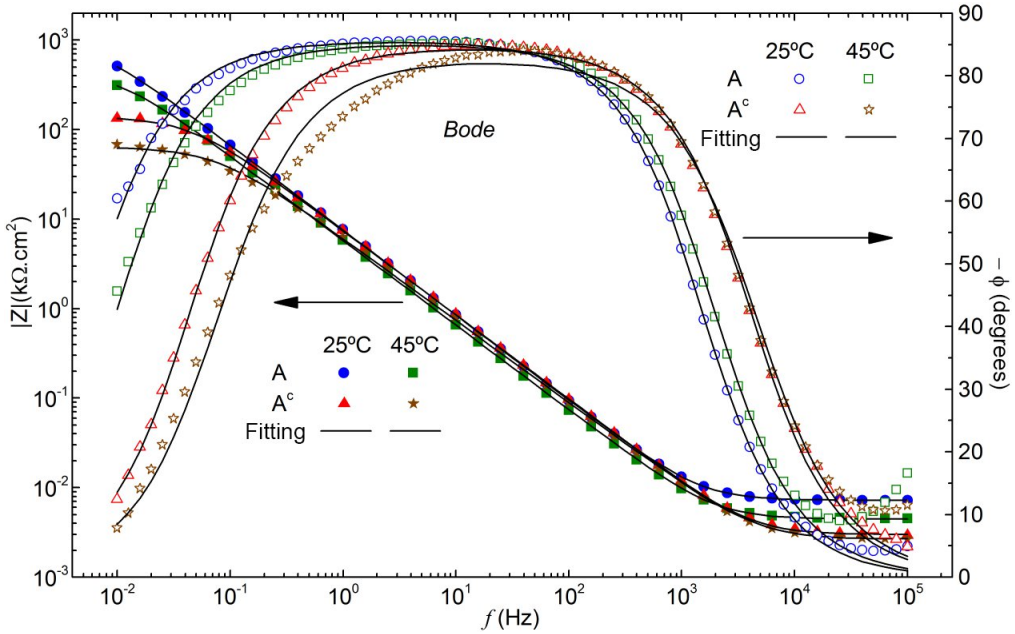

Figure 8: Bode diagrams and curves fitted by equivalent electrical circuit of alloys A and A^c at 25 and 45 °C

It should be noted that all samples present a wide range of frequencies in which the phase angle remains approximately constant, as predicted by the CPE (Constant Phase Element) behavior. Furthermore, it can be seen from the solid lines in the diagrams, that the circuit response was able to fit, with a good approximation, the electrochemical impedance spectroscopy data. In the Nyquist diagram, a qualitative analysis of the polarization resistance of the samples can be carried out by evaluating the radii of the semicircles formed. The amorphous alloys presented diagrams considerably larger than the crystalline alloys, revealing their greater resistance to corrosion. Moreover, increasing temperature reduces the polarization resistance of amorphous and crystalline alloys. These results agree with those obtained in the potentiodynamic polarization curves. The equivalent electrical circuit used to fit the experimental diagrams is shown in Figure 9.

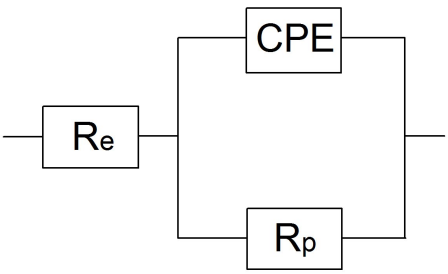

Figure 9: Equivalent electric circuit: Re represents the electrolyte resistance, Rp the polarization resistance and CPE the constant phase element.

Within the amorphous alloys, the Nyquist diagrams reveal that the polarization resistance values have the following decreasing order: C, B and A. This behavior occurs at both temperatures tested. In crystalline alloys, this order is reversed at the temperature of 25 °C, and at 45 °C, it is given by B^c, C^c and A^c. Observing Figures 6 and 7, the lower the value of the i_{pass} passivation current density, the greater the value of the polarization resistance (Rp).

Among the amorphous alloys containing boron, the one with the highest percentage of niobium (alloy C) presented the highest Rp, suggesting an increase in corrosion resistance due to the increase in the percentage of niobium, an effect contemplated in the literature [15,16]. In crystalline alloys, the effect of adding boron was exactly the opposite of what occurred in amorphous alloys, that is, the presence of boron reduced the polarization resistance of crystalline samples.

4 Conclusions

Using electrochemical techniques, it was possible to characterize the samples and demonstrate the superiority of amorphous alloys in relation to crystalline alloys for the same chemical composition, with the alloys and conditions studied. Using polarization curves, it was possible to demonstrate that glassy metals had a much lower passivation current density than their crystalline counterparts. Furthermore, electrochemical impedance spectroscopy data adjusted by an equivalent electrical circuit showed that the polarization resistance of the amorphous alloy was up to 20 times that of the crystalline one for the same chemical composition. The increase in temperature, from 25 °C to 45 °C, reduced the corrosion resistance of all studied alloys, especially the amorphous ones, which showed greater sensitivity to thermal effects than the crystalline ones. This increase in temperature, however, is low enough to promote structural changes in amorphous alloys.

For amorphous alloys, the presence of boron in ternary ones increased the polarization resistance and reduced the passivation current density, both at 25 °C and 45 °C in relation to the binary alloy without this element. Among the ternary amorphous alloys, the higher percentage of niobium also improved the corrosion resistance properties of the samples at the two temperatures used.

In crystalline alloys, the polarization curves and electrochemical impedance data revealed the greater corrosion resistance of the binary alloy in relation to the ternary compositions, when tested at 25 °C. However, increasing the temperature to 45 °C changed this behavior, suggesting that the presence of boron improves the resistance of crystalline alloys in relation to the thermal effect.

Acknowledgments

The authors would like to thank FAPERJ (Fundação Carlos Chagas Filho de Amparo à Pesquisa do Estado do Rio de Janeiro) for the financial assistance, CNPq, and InovUerj for the support with a Qualitec scholarship holder in the project. This study was financed in part by the Coordenação de Aperfeiçoamento de Pessoal de Nível Superior – Brasil (CAPES) – Finance Code 001.

References

[1] J. S. Andrade, I. N. Bastos, and L. C. R. Aliaga, “Determinação das características estruturais e mecânicas da liga de alta entropia Hf-Nb-Ta-Zr,” *Vetor*, vol. 30, no. 2, pp. 22–32, 2021. Available at: https://doi.org/10.14295/vetor.v30i2.13090

[2] K. Zheng, Z. He, L. Che, H. Cheng, M. Ge, T. Si, and X. Xu “Deep alloys: Metal materials empowered by deep learning,” *Materials Science in Semiconductor Processing*, vol. 179, p. 108514, 2024. Available at: https://doi.org/10.1016/j.mssp.2024.108514

[3] S. Xie, J. Zhao, S. Li, and J. Su, “Enhanced mechanical properties of Zr-Cu-Al-Ni bulk amorphous alloys by Ag and O doping,” *Journal of Alloys and Compounds*, vol. 957, p. 170186, 2023. Available at: https://doi.org/10.1016/j.jallcom.2023.170186

[4] H. Sonomura, K. Katagiri, T. Ozaki, Y. Hasegawa, T. Tanaka, and A. Kakitsuji, “In-situ preparation of Zr-Al-Ni-Cu amorphous alloy by friction stirring using a tool consisting of multiple metal foils,” *Materials Letters*, vol. 353, p. 135264, 2023. Available at: https://doi.org/10.1016/j.matlet.2023.135264

[5] S. F. Guo, H. J. Zhang, Z. Liu, W. Chen, and S. F. Xie, “Corrosion resistances of amorphous and crystalline Zr-based alloys in simulated seawater,” *Electrochemistry Communications*, vol. 24, pp. 39–42, 2012. Available at: https://doi.org/10.1016/j.elecom.2012.08.006

[6] H. Zhang, C. Zhang, B. Han, J. Qiu, H. Li, S. Qin, J. Liu, Y. Wang, P. Zhang, Y. Pan, and H. Zhou “Evolution of grain boundary character distributions in a cold-deformed Nickel-based superalloy during electropulsing treatment,” *Journal of Materials Research and Technology*, vol. 9, no. 3, pp. 5723–5734, 2020. Available at: https://doi.org/10.1016/j.jmrt.2020.03.097

[7] C.-Y. Lee, T.-J. Lin, H.-H. Sheu, and H.-B. Lee, "A study on corrosion and corrosion-wear behavior of Fe-based amorphous alloy coating prepared by high velocity oxygen fuel method," *Journal of Materials Research and Technology*, vol. 15, pp. 4880–4895, 2021. Available at: https://doi.org/10.1016/j.jmrt.2021.10.103

[8] H. Alves and U. Heubner, "Aqueous Corrosion of Nickel and its Alloys," in *Shreir's Corrosion*, vol. 3, 2010, pp. 1879–1915. Elsevier eBooks. Available at: https://doi.org/10.1016/b978-044452787-5.00092-5

[9] C. Suryanarayana and A. Inoue, *Bulk Metallic Glasses*, 2nd edition, 2017.

[10] L. Xia, W. H. Li, S. S. Fang, B. C. Wei, and Y. D. Dong, "Binary Ni–Nb bulk metallic glasses," *Journal of Applied Physics*, vol. 99, no. 2, 2006. Available at: https://doi.org/10.1063/1.2158130

[11] W. J. Botta, J. E. Berger, C. S. Kiminami, V. Roche, R. P. Nogueira, and C. Bolfarini, "Corrosion resistance of Fe-based amorphous alloys," *Journal of Alloys and Compounds*, vol. 586, pp. S105–S110, 2014. Available at: https://doi.org/10.1016/j.jallcom.2012.12.130

[12] G.Y. Koga, R.P. Nogueira, V. Roche, A.R. Yavari, A.K. Melle, J. Gallego, C. Bolfarini, C.S. Kiminami, W.J. Botta, "Corrosion properties of Fe–Cr–Nb–B amorphous alloys and coatings," *Surface & Coatings Technology*, vol. 254, pp. 238–243, 2014. Available at: https://doi.org/10.1016/j.surfcoat.2014.06.022

[13] A. Fattah-Alhosseini, F. Soltani, F. Shirsalimi, B. Ezadi, and N. Attarzadeh, "The semiconducting properties of passive films formed on AISI 316 L and AISI 321 stainless steels: A test of the point defect model (PDM)," *Corrosion Science*, vol. 53, no. 10, pp. 3186–3192, 2011. Available at: https://doi.org/10.1016/j.corsci.2011.05.063

[14] K. Park, S. Ahn, and H. Kwon, "Effects of solution temperature on the kinetic nature of passive film on Ni," *Electrochimica Acta*, vol. 56, no. 3, pp. 1662-1669, 2011. Available at: https://doi.org/10.1149/ma2012-02/22/2179

[15] C. Qin, W. Zhang, H. Kimura, K. Asami, and A. Inoue, "New Cu-Zr-Al-Nb Bulk Glassy Alloys with High Corrosion Resistance," *Materials Transactions*, vol. 45, no. 6, pp. 1958–1961, 2004. Available at: https://doi.org/10.2320/matertrans.45.1958

[16] S.-J. Pang, C.-H. Shek, T. Zhang, K. Asami, and A. Inoue, "Corrosion behavior of glassy Ni55Co5Nb20Ti10Zr10 alloy in 1N HCl solution studied by potentiostatic polarization and XPS," *Corrosion Science*, vol. 48, no. 3, pp. 625–633, 2006. Available at: https://doi.org/10.1016/j.corsci.2005.02.013